Molecular Cell *23*, 457–469, August 18, 2006 ©2006 Elsevier Inc. DOI 10.1016/j.molcel.2006.06.019

Double-Stranded DNA Translocation: Structure and Mechanism of Hexameric FtsK

Thomas H. Massey,[2,3] Christopher P. Mercogliano,[1,3] James Yates,[2] David J. Sherratt,[2] and Jan Löwe[1,*]
[1] MRC Laboratory of Molecular Biology
Hills Road
Cambridge CB2 2QH
United Kingdom
[2] Division of Molecular Genetics
Department of Biochemistry
University of Oxford
South Parks Road
Oxford OX1 3QU
United Kingdom

Summary

FtsK is a DNA translocase that coordinates chromosome segregation and cell division in bacteria. In addition to its role as activator of XerCD site-specific recombination, FtsK can translocate double-stranded DNA (dsDNA) rapidly and directionally and reverse direction. We present crystal structures of the FtsK motor domain monomer, showing that it has a RecA-like core, the FtsK hexamer, and also showing that it is a ring with a large central annulus and a dodecamer consisting of two hexamers, head to head. Electron microscopy (EM) demonstrates the DNA-dependent existence of hexamers in solution and shows that duplex DNA passes through the middle of each ring. Comparison of FtsK monomer structures from two different crystal forms highlights a conformational change that we propose is the structural basis for a rotary inchworm mechanism of DNA translocation.

Introduction

Prokaryotes have dedicated motor proteins with conserved RecA-like domains for pumping DNA between cellular loci (and sometimes across membranes) in cell division, viral DNA packaging, conjugation, and sporulation. Some of these DNA translocases (e.g., TrwB, which is involved in bacterial conjugation; [Gomis-Rüth et al., 2001]) act on single-stranded DNA and bear structural resemblance to the family of ring helicases that includes T7gp4, DnaB, and the SV40 large T antigen (for review see Patel and Picha [2000]). The remainder act on dsDNA and include SpoIIIE and FtsK. SpoIIIE moves chromosomal DNA from the mother cell to prespore prior to sporulation in *Bacillus subtilis* (Bath et al., 2000), whereas FtsK acts in the late stages of chromosome segregation at the closing division septum in *Escherichia coli* and most other eubacteria.

FtsK is a multidomain protein with roles in chromosome decatenation and segregation, dimer resolution, and cell division (Liu et al., 1998; Capiaux et al., 2001; Ip et al., 2003). The 1329 residue protein from *E. coli* can be divided into three domains: a membrane-spanning N-terminal domain ($FtsK_N$) essential for cell division, a long 600 residue proline/glutamine rich linker, and a 512 residue C-terminal ATPase domain ($FtsK_C$; [Yu et al., 1998; Barre et al., 2000; Aussel et al., 2002]). This general domain structure is common to all FtsK proteins identified, although the linker varies significantly in length and composition despite being essential in *E. coli* for normal chromosomal *dif* recombination and cell division (Boyle et al., 2000; Bigot et al., 2004). Fluorescent microscopy has shown that $FtsK_N$ localizes the protein to the nascent division septum of *E. coli*, thus positioning the protein for its coordinating role in cell division and chromosome segregation (Barre et al., 2000; Wang et al., 2005). $FtsK_C$ has been classified by primary sequence as a member of the RecA-like family of ATPases. Many of these enzymes function as oligomers and often form rings with nucleotide binding pockets between subunits (e.g., hexameric helicases; [Patel and Picha, 2000; Iyer et al., 2004]). Biochemical assays with an oligomeric derivative of the *E. coli* C-terminal domain ($FtsK_{50C}$) have shown that $FtsK_C$ is a DNA-dependent ATPase with two distinct roles: translocation of dsDNA at speeds of up to 6.7 kbp/s, and activation of XerCD site-specific recombination at *dif* such that chromosome dimers, which may arise as a consequence of homologous recombination on circular DNAs, can be resolved to monomers prior to cell division (Aussel et al., 2002; Massey et al., 2004; Saleh et al., 2004; Pease et al., 2005). Single-molecule studies have shown that FtsK can translocate rapidly toward *dif* on dsDNA, and recent experiments have identified a polar 8 bp sequence element (KOPS) that directs FtsK translocation independently of any accessory factors (Pease et al., 2005; Bigot et al., 2005). Individual FtsK particles can translocate bidirectionally, enabling them to reverse direction if they encounter a KOPS in nonproductive orientation (Saleh et al., 2004; Pease et al., 2005). The polarity of KOPS elements switches precisely at *dif* in the *E. coli* chromosome to ensure that FtsK translocation is always directed toward the recombination site. Because FtsK is tethered at the division septum, DNA translocation will bring sister *dif* regions of segregating chromosomes to midcell. If a chromosome dimer or catenane is present in the cell, such translocation will facilitate *dif* sites synapsis near the septum, where FtsK is perfectly positioned to contact XerD and thereby stimulate dimer/catenane-resolving recombination.

$FtsK_C$ can be subdivided into three separate domains (α, β, and γ; Figure 1A) on the basis of secondary structure prediction. "Mix and match" experiments between *Haemophilus influenzae* and *E. coli* Xer/FtsK, and the exploitation of FtsK chimeras containing different subdomains of *H. influenzae* and *E. coli* $FtsK_C$ showed that the γ domain of $FtsK_C$ interacts directly with the recombination machinery in order to activate dimer resolution, whereas α and β contain the core ATPase machinery (Yates et al., 2003). Biochemical data indicate that γ interacts directly with XerD for recombinase activation (Yates et al., 2006).

*Correspondence: jyl@mrc-lmb.cam.ac.uk
[3] These authors contributed equally to the work.

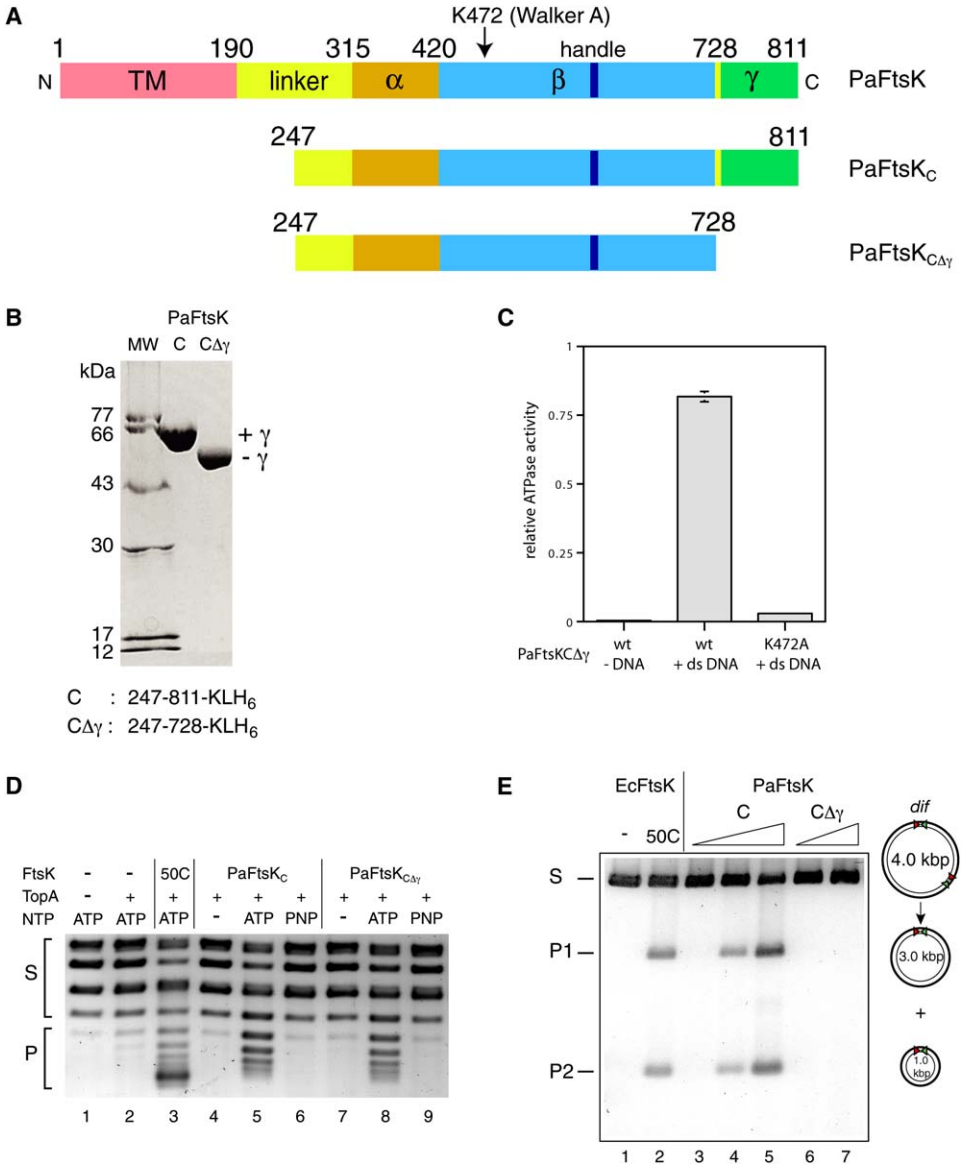

Figure 1. Purification and Activities of FtsK$_C$ Derivatives from *Pseudomonas aeruginosa*

(A) Domain architecture of PaFtsK. Top shows the full-length protein, with the N-terminal transmembrane (TM) domain attached to FtsK$_C$ through a short (125 amino acid) linker. FtsK$_C$ consists of three subdomains, α, β, and γ, of which α and β constitute the DNA translocase and γ interacts with XerD (Yates et al., 2006). The "handle" is 13 contiguous amino acids (570–582) in the β domain implicated in dodecamer formation (Figure 4). The bottom two schematics show the PaFtsK$_C$ derivatives, with (middle) and without (bottom) γ, used in this study.

(B) SDS-PAGE of PaFtsK proteins used in this study. Proteins were overexpressed in *E. coli* and purified by using nickel affinity, size exclusion, and anion exchange chromatography. The absence of γ in PaFtsK$_{C\Delta\gamma}$ compared to PaFtsK$_C$ is clearly observed.

(C) ATPase activities of wild-type and K472A (Walker A mutant) PaFtsK$_{C\Delta\gamma}$ in the presence and absence of 30 bp dsDNA. The chart shows the mean ± SD for three independent experiments. The assay is saturated, and readout is nonlinear because of the very fast ATPase rate of FtsK when stimulated by DNA.

(D) PaFtsK$_C$ and PaFtsK$_{C\Delta\gamma}$ can translocate dsDNA in the presence of ATP. An array of partially relaxed pUC19 topoisomers (S; lane 1) was incubated on ice with EcFtsK$_{50C}$ (lane 3), PaFtsK$_C$ (lanes 4–6), or PaFtsK$_{C\Delta\gamma}$ (lanes 7–9) in the presence of TopA (from *E. coli*, to remove negative supercoils induced by DNA translocation) and NTP where indicated (PNP = AMP-PNP, a nonhydrolysable analog of ATP). All three derivatives of FtsK are able to translocate DNA, as indicated by the appearance of plectonemic (P) positive supercoiling, but only in the presence of hydrolysable ATP.

(E) PaFtsK$_C$, but not PaFtsK$_{C\Delta\gamma}$, can stimulate Xer site-specific recombination by *E. coli* XerCD on a plasmid dimer substrate (pSDC124) containing two *dif* sites in direct repeat. Xer recombination on pSDC124 (4.0 kbp) resolves the plasmid into two smaller plasmid products (3.0 kbp and 1.0 kbp), and this reaction requires XerCD, active FtsK, and ATP. *E. coli* FtsK$_{50C}$ is shown as a positive control (lane 2). PaFtsK$_C$ stimulates pSDC124 resolution in a concentration-dependent manner (0.3, 1.0, and 3.0 μM monomer in lanes 3, 4, and 5, respectively), whereas PaFtsK$_{C\Delta\gamma}$ (1.0 and 3.0 μM monomer in lanes 6 and 7, respectively) cannot support recombination as it lacks a γ domain.

We present structures of $FtsK_C$ derivatives from *E. coli* and *Pseudomonas aeruginosa*. The protein forms hexameric rings that can pair head to head to form double rings. EM and analytical ultracentrifugation show that rings form only in the presence of DNA and indicate that dsDNA passes through the center of the rings. Structures of FtsK monomers from two oligomeric forms (dimer and hexamer) of *P. aeruginosa* $FtsK_C$ highlight a conformational change that suggests a rotary inchworm mechanism for dsDNA translocation by FtsK.

Results and Discussion

Construction of FtsK Derivatives for Structural Studies

Previous biochemical studies of FtsK have focused on $FtsK_{50C}$, an oligomeric derivative of $FtsK_C$ from *E. coli* (Aussel et al., 2002; Massey et al., 2004; Saleh et al., 2004; Pease et al., 2005). Although this protein has ATP-dependent DNA translocation and XerD-activating activities, it is unsuitable for structural studies due to its low solubility and tendency to aggregate. $FtsK_C$ protein from *E. coli* ($EcFtsK_C$) is also unsuitable for structural work due to its toxicity when overexpressed. To circumvent these problems, an ATPase mutant of $EcFtsK_C$ (K997A in the Walker A motif) was purified in large quantities: it was very soluble but monomeric and lacking all ATPase-associated activities. Nevertheless, we determined the structure of this mutant by X-ray crystallography and noted the distinct α and β domains of the protein, with a cleft between them (see below). However, the γ domain responsible for XerD interaction was not observed. HSQC NMR data on the isolated γ domain show that it is structured (Figure S1 in the Supplemental Data available with this article online), and thus, its invisibility in the crystal structure is presumably due to the flexibility of the short glycine-rich linker joining it to the rest of the protein.

Alignment of many FtsK proteins showed that the linker between N- and C- terminal domains varies in length and composition (data not shown). We reasoned that an FtsK protein with a short linker might be more amenable to structural investigation than engineered derivatives of *E. coli* FtsK (like $FtsK_{50C}$), which are missing the majority of a long, 600 residue, linker region, especially given that the EcFtsK linker is required for full chromosome dimer resolution activity in vivo (Bigot et al., 2004). FtsK from *Pseudomonas aeruginosa* had the shortest linker (~125 residues), and we thus cloned and purified a derivative consisting of 68 residues of linker and the full C-terminal domain ($PaFtsK_C$; Figure 1A). We also prepared a derivative of $PaFtsK_C$ without a γ domain ($PaFtsK_{C\Delta\gamma}$) in the expectation that such a protein might form more stable oligomers and crystallize more easily (Figures 1A and 1B). Both His-tagged proteins could be prepared in large amounts at high concentration without solubility problems, in contrast to $FtsK_{50C}$ from *E. coli*.

$PaFtsK_C$ Hydrolyzes ATP, Translocates dsDNA, and Activates XerCD Recombination

Purified $PaFtsK_C$ and $PaFtsK_{C\Delta\gamma}$ are robust DNA-dependent ATPases (Figure 1C). ATPase activities were strictly protein concentration dependent, correlating with a cooperative monomer to hexamer transition at ~1 μM (monomer; data not shown). These proteins can also translocate dsDNA, as measured by supercoil induction in a relaxed plasmid (Figure 1D). Interestingly, strong translocation activities comparable to $EcFtsK_{50C}$ were only observed in the presence of Ni-NTA beads, perhaps because the beads were necessary for constraining the low levels of supercoil induction. $FtsK_C$ proteins from *E. coli* and *P. aeruginosa* are 59.6% identical by primary sequence, making it reasonable to expect $PaFtsK_C$ to be able to activate Xer site-specific recombination by *E. coli* recombinases between *E. coli dif* sites. $PaFtsK_C$, but not $PaFtsK_{C\Delta\gamma}$, could activate Xer recombination in a heterologous (*E. coli*) in vitro plasmid dimer resolution assay (Figure 1E; Aussel et al., 2002). The failure of $PaFtsK_{C\Delta\gamma}$ to activate Xer recombination presumably arose from its inability to interact productively with XerD, due to the absence of γ (Yates et al., 2006). These data indicate that the purified PaFtsK derivatives translocate DNA and activate recombination in a comparable manner to $FtsK_{50C}$ from *E. coli*.

$PaFtsK_C$ Forms Hexameric Rings in the Presence of DNA

EM showed that both $PaFtsK_C$ and $PaFtsK_{C\Delta\gamma}$ form hexameric rings in the presence of short (15–30 bp) dsDNA (Figure 2A). Ring formation was dependent on DNA, but not on nucleotide or magnesium ions. Rings were always hexameric and uniform in size and structure, with an outer diameter of ~120 Å and an inner diameter of ~30 Å.

Analytical ultracentrifugation (AUC) of $PaFtsK_{C\Delta\gamma}$ with and without DNA reinforced the EM data. Without DNA, the protein existed as a monomer, irrespective of the presence or absence of nucleotide and magnesium ions. Addition of 15 bp DNA duplex converted more than 98% of the monomers into hexamers (Figure 2B). Robust hexamer formation in AUC (as in EM) was protein concentration dependent, requiring at least 10 μM monomer (Figure 2B, bottom).

A similar DNA dependence of translocase assembly has been deduced from in vivo data in *B. subtilis* for SpoIIIE (Ben-Yehuda et al., 2003).

$PaFtsK_{C\Delta\gamma}$ Can Form Linear Arrays of Hexameric Rings on DNA

All EM images of $PaFtsK_{C\Delta\gamma}$ with 30 bp DNA show fields of mostly face-on hexamers (Figure 2A). To visualize rings from the side, different lengths of dsDNA ranging from 55 to 625 bp were incubated with saturating concentrations of $PaFtsK_{C\Delta\gamma}$ (Figure 2C). Side views of individual rings were clearly defined, and the number of rings bound per DNA was directly proportional to the length of that DNA (Figure 2C). Each ring covered 39.9 bp (136 Å) of DNA, this figure including the space between rings as well as the footprint of the protein.

In order to visualize DNA and protein simultaneously, samples of DNA with or without saturating $PaFtsK_{C\Delta\gamma}$ were lightly negatively stained, rotary shadowed, and viewed by EM (Figure 2D). There was no significant difference in DNA length with or without protein (Figure 2D, right) before and after incubation with a saturating concentration of $PaFtsK_{C\Delta\gamma}$. Together, these data indicate that DNA binding by $PaFtsK_{C\Delta\gamma}$ does not occur

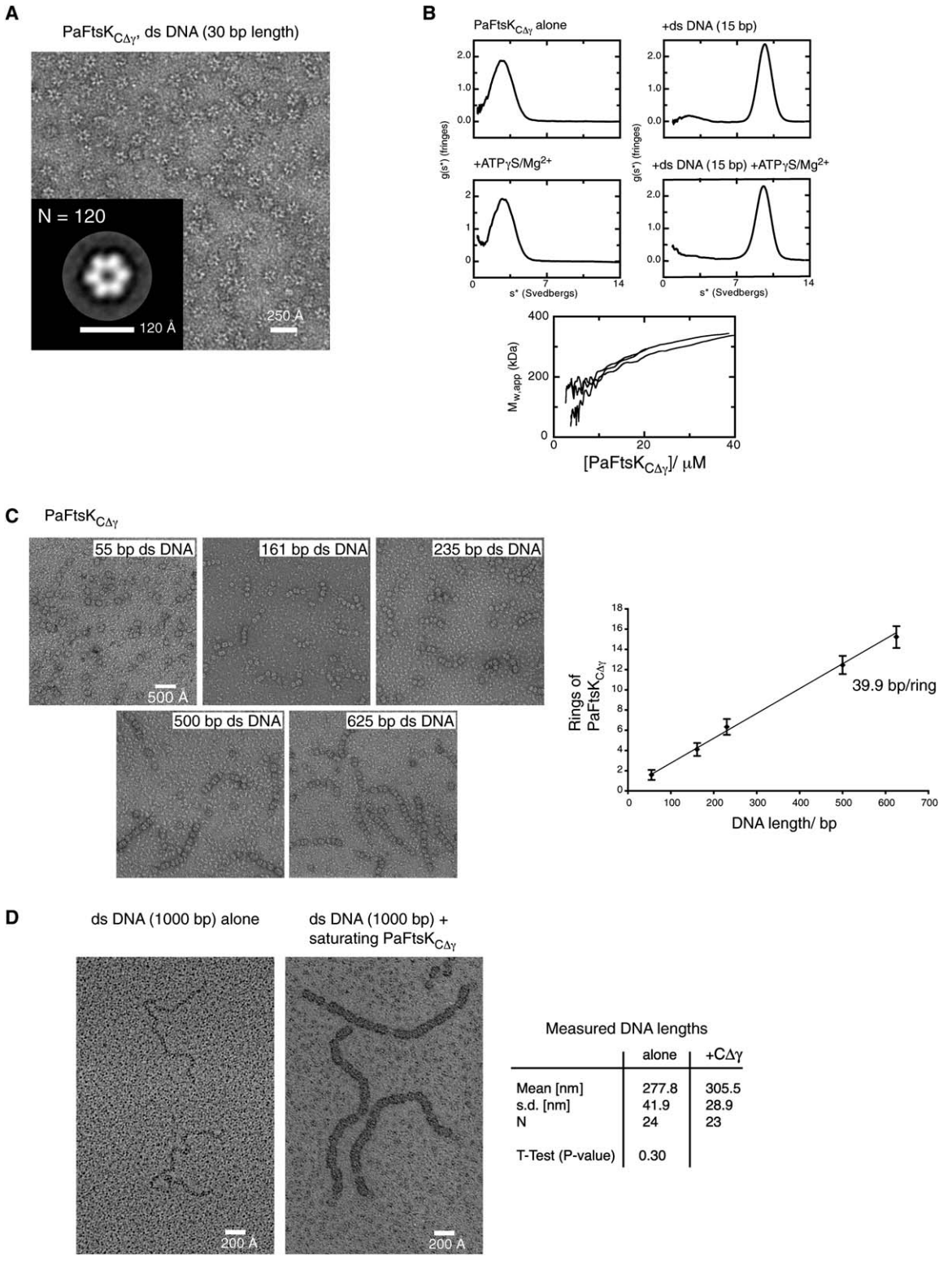

Measured DNA lengths

	alone	+CΔγ
Mean [nm]	277.8	305.5
s.d. [nm]	41.9	28.9
N	24	23
T-Test (P-value)	0.30	

Figure 2. PaFtsK$_{C\Delta\gamma}$ Forms Hexameric Rings around DNA

(A) Electron micrograph of negatively stained PaFtsK$_{C\Delta\gamma}$ (280 nM hexamer) after 2 min incubation on ice with dsDNA (420 nM; 30 bp length), ATPγS (2 mM), and MgOAc (4 mM). The main class average with 120 particles clearly shows a hexameric ring of 120 Å diameter with a channel (~30 Å diameter) on the inside.

(B) Analytical ultracentrifugation confirms hexamer formation in the presence of dsDNA. PaFtsK$_{C\Delta\gamma}$ (20 μM monomer) exists as monomer in the presence or absence of ATPγS/MgOAc (2 mM/4 mM; top left panels). Addition of DNA converts >98% of the protein into a hexameric form, whether or not ATPγS/MgOAc is present (top right panels). Graphs of PaFtsK$_{C\Delta\gamma}$ concentration against mean particle molecular weight from three equilibrium runs (bottom) show that only at high protein concentrations (>10 μM) is most of the PaFtsK$_{C\Delta\gamma}$ in hexameric form.

by wrapping, looping, or another mechanism that would alter DNA length but probably involves threading DNA through the central hole of the ring.

Monomeric FtsK$_C$ Has a Structure Related to RecA and DNA/RNA-Helicases/Pumps

The structure of monomeric K997A (Walker A mutant) FtsK$_C$ from *E. coli* was determined to 2.7 Å by X-ray crystallography from crystals containing head-to-tail dimers of the protein (Figure 3A and Tables 1 and 2). The monomer structure consisted of two domains (α and β) with a distinctive cleft between them, connected by two β strands. The γ domain was disordered. The structure of the α domain, or jaw, is unique to FtsK, whereas the β domain has the archetypal RecA-like fold that is common to many oligomeric ATPases, including T7 gp4 and related hexameric helicases, TrwB, and F1. Structurally, TrwB bears the closest relation to FtsK$_C$, although the α domains are very different (DALI; Holm and Sander, 1995). Another version of FtsK$_C$ from *P. aeruginosa* (PaFtsK$_C$) containing the α, β, and γ domains only was also crystallized in the same head-to-tail dimer form except this structure contained two molecules of ATPγS (Figure 3A, right). The structure was solved to 2.25 Å by molecular replacement using the structure of the *E. coli* protein as a model. The FtsK$_C$ monomer structures from *E. coli* and *P. aeruginosa* are very similar (rmsd 0.98 Å, 64% sequence identity, 93% Cα aligned), each having distinct α and β domains and an unobserved γ domain (Figure 3A, left). The PaFtsK$_C$ structure shows how the β domain of a monomer binds nucleotide and also highlights a structured 13 residue loop ("handle") that extends out of β from the side furthest from α. The relevance of the head-to-tail dimer structure found in both crystal forms of FtsK$_C$ is unknown (Figure 3A, right).

PaFtsK$_{C\Delta\gamma}$ Crystallizes as a Hexamer, with a Large 30 Å Diameter Channel

Monomeric FtsK$_C$ lacks ATPase, DNA translocase, or recombinase-stimulating activities in vitro (Aussel et al., 2002; data not shown). In order to obtain the structure of a functional form of FtsK$_C$, we crystallized PaFtsK$_{C\Delta\gamma}$, as EM and AUC showed this protein forms stable rings in solution (Figure 2). The protein crystallized as a hexamer, which was solved to 2.9 Å by molecular replacement (Tables 1 and 2) and consisted of a closed ring of 120 Å outer diameter with a central annulus of ~30 Å diameter (measured between van der Waal's surfaces; Figure 3B). Face on, the structure fits closely with the averaged EM view of a hexamer (Figure 2A). The side view of the hexamer shows that it approximates a truncated cone, consisting of two clearly defined parts separated by a cleft of ~10 Å: a ring formed by the six α subunits and a larger ring formed by the six β subunits (Figure 3B, left). The six handles are observed protruding from the open side of the β ring. There are five main loops lining the channel that could contact DNA: two in α (300–302 and 380–384) and three in β (606–610, 633–640, and 655–673).

PaFtsK$_{C\Delta\gamma}$ was crystallized in the presence of ATPγS and magnesium ions. The structure contains predominantly ADP, indicating that most of the ATPγS has been hydrolyzed over the course of the crystallization. Each active site of the enzyme resembles a typical RecA nucleotide binding site with all the residues of a particular active site belonging to a single monomer within the ring (Figure 3C). This arrangement is akin to that found in TrwB and F1 but in contrast to many other hexameric ATPases (e.g., T7 gp4, SV40 large T antigen, and RepA) where the active site is formed between two subunits with residues (such as the "arginine finger") being contributed by both protomers (Singleton et al., 2000; Niedenzu et al., 2001; Li et al., 2003). However, an arginine in PaFtsK (R620) has been identified in sequence alignments as the equivalent of the arginine finger (Iyer et al., 2004). This residue is 10.5 Å from the β-phosphate of the nucleotide and thus too distant to be involved in catalysis in the protein conformation crystallized here. However, we believe the residue may be close enough to join the active site in an asymmetric, DNA bound form of the hexamer.

The nucleotide is positioned such that it makes contact with residues (E596 and Q631) that are linked directly to two loops (606–610 and 633–640, respectively) that line the inside of the channel in the center of the hexamer. This contact between the nucleotide and parts of the protein that may bind DNA fits a mechanism of nucleotide-dependent DNA binding and release that could lead to translocation.

The Central Channel Is Large Enough to Accommodate dsDNA

The central channel of the PaFtsK$_{C\Delta\gamma}$ hexamer is ~30 Å in diameter and ~60 Å in length (Figures 3B and 3D). Modeling B-DNA into the structure indicates that the channel is precisely the right diameter for accommodating a DNA duplex, that the α and β domains may contact the DNA duplex almost exactly one turn apart (through loop 380–384 in α and loop 633–640 in β), and that there is no obvious steric impediment to rapid DNA translocation (Figure 3D, left and middle). One or two (diametrically opposed) subunits may contact DNA at any given time. A comparison between hexameric ring proteins that act on ssDNA (e.g., TrwB and T7 gp4 helicase; [Singleton et al., 2000; Gomis-Rüth et al., 2001]) and the structure of PaFtsK$_{C\Delta\gamma}$ presented here highlights the difference in diameter of the central channel (Figure 3D, right). The channel of FtsK has a much greater diameter, as it must accommodate and act on dsDNA and is similar in dimensions to the central channel of the eukaryotic sliding clamp, PCNA, that also embraces a DNA duplex (Figure 3D, right; Krishna et al., 1994).

PaFtsK$_{C\Delta\gamma}$ Can Form Double Rings Threaded on DNA

Viewing dsDNA (1000 bp) with a subsaturating concentration of PaFtsK$_{C\Delta\gamma}$ by EM after prolonged incubation, light negative staining, and rotary shadowing indicated

(C) PaFtsK$_{C\Delta\gamma}$ coats DNAs of different length and occupies 39.9 bp per ring on average. dsDNAs of different lengths (55, 161, 230, 500, and 625 bp) were incubated with saturating concentrations of protein, negatively stained, and viewed by EM. The number of rings binding to each DNA was counted and plotted against DNA length (right). At least 550 rings were counted for each DNA length, and means ± SD are plotted.
(D) DNA length is unchanged by PaFtsK$_{C\Delta\gamma}$ binding, as shown by comparison of shadowed samples of 1000 bp dsDNA with saturating (right) and without (left) PaFtsK$_{C\Delta\gamma}$.

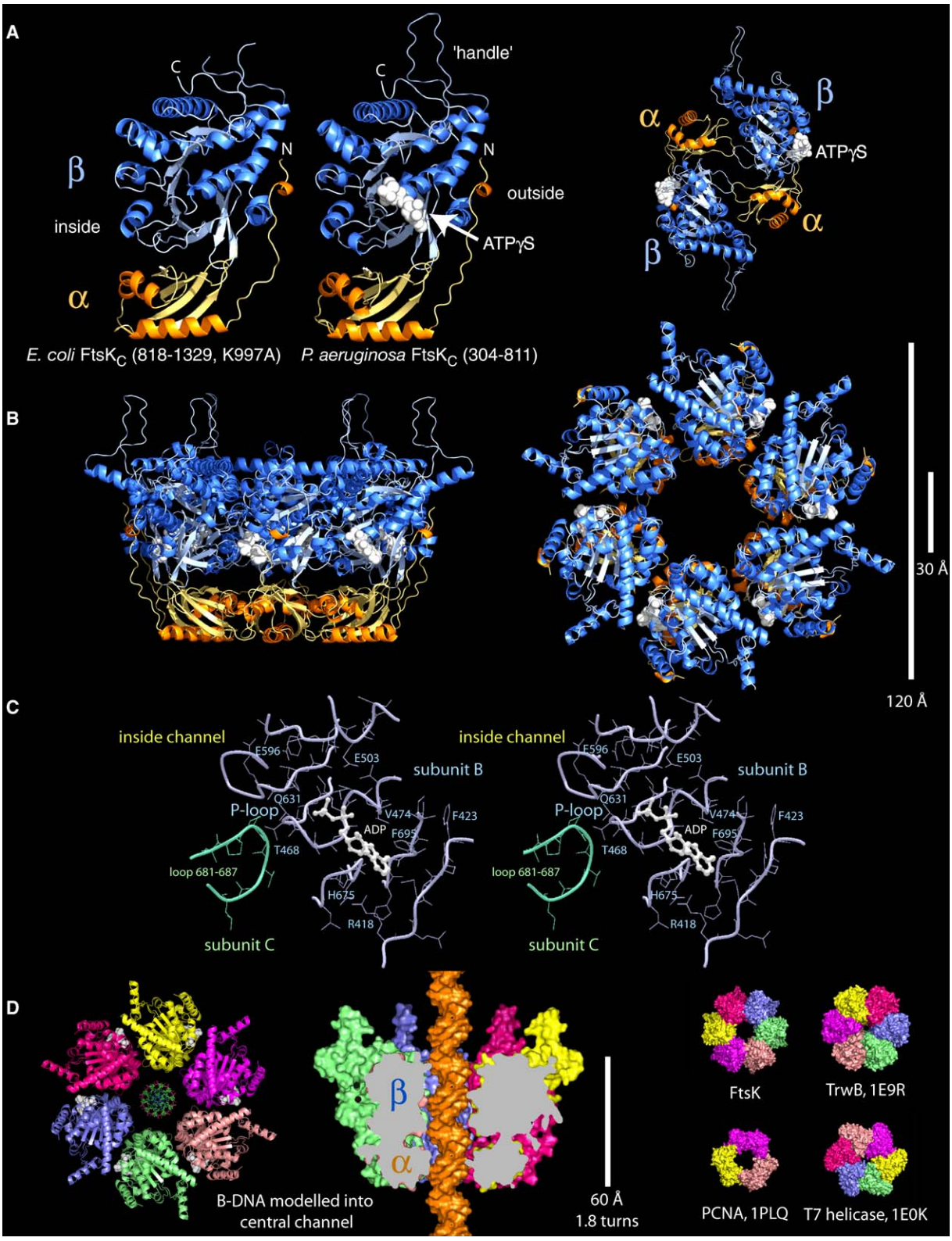

Figure 3. Crystal Structures of FtsK

(A) Crystal structures of FtsK$_C$ from *E. coli* (left) and *P. aeruginosa* (middle). FtsK$_C$ contains two domains (α and β): the α domain being unique to FtsK, and the β domain being RecA related. Based on the hexameric structure (B), the inside of the channel is to the left in the orientation shown. A head-to-tail dimer (right) was found in several crystal forms of FtsK$_C$ from both *E. coli* and *P. aeruginosa*.

(B) Crystal structure of hexameric PaFtsK$_{C\Delta\gamma}$ viewed from the side (left) and top (right). Six subunits form a closed ring with an outer diameter of ~120 Å and a central channel of ~30 Å diameter. Nucleotide binding sites are near the outside of the ring, close to, but not in, an intersubunit contact.

Table 1. Crystallographic Data

Crystal	λ[Å]	Resolution [Å]	I/σI[a]	Rm[b] [%]	Multiplicity[c]	Completeness [%][d]
EcFtsK:	*E. coli* $FtsK_C$ (818–1329, K997A, no tag) SeMet, P3(2), a = b = 174.5 Å, c = 119.8 Å					
PEAK1	0.9793	3.5	12.3(4.6)	0.081(0.230)	3.4(3.2)	99.5(98.5)
INFL1	0.9797	3.5	12.8(4.6)	0.083(0.241)	3.7(3.4)	99.8(99.1)
REM1	0.9184	3.5	11.9(4.2)	0.086(0.253)	3.5(3.2)	99.3(98.1)
PEAK2	0.9793	3.5	12.4(4.6)	0.091(0.262)	3.9(3.7)	98.8(99.3)
INFL2	0.9797	3.5	12.2(4.4)	0.092(0.272)	3.9(3.7)	98.8(99.3)
REM2	0.9184	3.5	11.2(4.0)	0.102(0.303)	3.9(3.7)	98.5(99.2)
	native, P2(1), a = 97.6 Å, b = 117.2 Å, c = 132.8 Å, β = 100.5°					
ECK	0.9790	2.7	11.3(3.9)	0.103(0.291)	3.7(3.8)	99.8(99.8)
PaFtsK:	*P. aeruginosa* $FtsK_C$ (304–811, KLH_6)					
	native, P1, a = 46.2 Å, b = 57.4 Å, c = 98.1 Å, α = 94.6°, β = 93.8°, γ = 107.7°					
PAK	0.9792	2.25	9.1(3.8)	0.081(0.337)	1.9(1.9)	93.8(93.3)
PaFtsK $_{C\Delta\gamma}$:	*P. aeruginosa* $FtsK_{C\Delta\gamma}$ (247–728, KLH_6)					
	ATPγS, P2(1)2(1)2, a = 140.0 Å, b = 221.8 Å, c = 134.1 Å					
PAKg	0.9340	2.9	13.1(3.3)	0.078(0.374)	3.7(3.7)	99.8(100)

[a] Signal to noise ratio for merged intensities (highest resolution bins in brackets).
[b] Rm: $\Sigma h \Sigma i |I(h,i) - I(h)| / \Sigma h \Sigma i\, I(h,i)$ where I(h,i) are symmetry-related intensities and I(h) is the mean intensity of the reflection with unique index h.
[c] Multiplicity for unique reflections, anomalous multiplicity in brackets.
[d] Completeness for unique reflections, anomalous completeness is identical because inverse beam geometry was used for MAD phasing.

the presence of double FtsK rings. Particle averaging showed that these double rings consist of two hexamers, head to head, with DNA running through the aligned central annuli (Figure 4A). These particles were further investigated by cryo-EM, enabling a 3D reconstruction of the double ring on DNA. The DNA clearly enters the center of one of the hexameric rings (Figure 4B). DNA is not observed on the other side of the dodecamer because its flexibility limits alignment of the DNA exiting the complex, necessitating a one-sided average.

The crystals containing hexameric rings also contained a distinctive dodecameric double ring structure formed by the head-to-head (β to β) arrangement of two individual hexamers (Figure 4C, left). This head-to-head arrangement contrasts with that in SV40 L-Tag and archaeal MCM dodecamers where the two nonmotor N-terminal domains interact (Fletcher et al., 2003; Li et al., 2003; McGeoch et al., 2005). The $FtsK_{C\Delta\gamma}$ double ring structure is ~150 Å in length, with a 10–20 Å gap at the interface between the two rings, fitting exactly with the EM observations. This gap is too small to accommodate even a distorted double helix. The interfacial interaction is mediated through the extended handles of β (residues 570–582 in PaFtsK), which were noted earlier in the monomer structure. Surprisingly, mutant versions of $PaFtsK_{C\Delta\gamma}$ and $PaFtsK_C$ lacking the handle (residues P570–P582 were deleted, leaving just a handle stump linking D569 to Q583; Figure 4C, right) were still able to form double rings effectively as were proteins lacking the His tags originally used for protein purification (data not shown). Hence, $PaFtsK_C$ has a propensity for forming double rings on DNA, with or without the aid of protein handles (or His tags). The relevance of the double rings remains unclear, although they could permit bidirectional DNA translocation by an individual FtsK dodecamer.

Inchworm-Type Translocation Is Suggested by an Interdomain Movement in $PaFtsK_C$

A comparison of monomers of $PaFtsK_C$ and $PaFtsK_{C\Delta\gamma}$, from the head-to-tail dimer (containing ATPγS; Figure 3A) and the full hexamer (containing ADP; Figure 3B), respectively, revealed a conformational change that is an almost pure, jaw-like, hinged movement (~12°) of the α domain with respect to the β domain. Jaw opening moves the channel-facing portion of α 5.5 Å away from β as well as withdrawing it slightly from the channel (Figure 5A). The cleft between α and β is thus central to this conformational change, allowing the spatial relationship between the two domains to change with nucleotide

(C) Stereo diagram of the active site of hexameric $PaFtsK_{C\Delta\gamma}$. The overall architecture resembles a RecA-like nucleotide binding site. In the hexamer crystallized, no residue from a neighboring subunit (green) contacts the nucleotide (white) directly. Two loops (containing Q631, E596) that can potentially sense the γ phosphate of the nucleotide reach into the channel of the hexamer where the DNA is translocated, suggesting a physical and functional link between nucleotide binding/hydrolysis and DNA translocation.
(D) The central channel in hexameric $PaFtsK_{C\Delta\gamma}$ can accommodate B form DNA. Left, top view of a $PaFtsK_{C\Delta\gamma}$ hexamer containing modeled B form DNA. Middle, cut-away side view of $PaFtsK_{C\Delta\gamma}$ containing modeled B form DNA (orange). Van der Waal's surfaces are shown to highlight the flush fit of dsDNA in the central channel of $FtsK_C$. The α and β domains contact dsDNA almost exactly one turn of the double helix apart. Right, comparison of hexamer structures and central channels of $PaFtsK_{C\Delta\gamma}$, PCNA, TrwB, and T7 gp4 helicase showing how only $PaFtsK_{C\Delta\gamma}$ and PCNA have a large enough annulus to accommodate dsDNA.

Table 2. Refinement Statistics

	$EcFtsK_C$	$PaFtsK_C$	$PaFtsK_{C\Delta\gamma}$
	Three Dimers	One Dimer	Hexamer
Model	Six chains A–F	Two chains A, B	Six chains A–F
	Residues 840–849, 858–1097, 1107–1248	Residues 315–722	Residues 315–722
		2 ATPγS	6 ADP
		2 magnesium	0 magnesium
	569 water molecules	365 water molecules	0 water molecules
Diff. data	ECK, 2.9 Å, all data	PAK, 2.25 Å, all data	PAKg, 2.9 Å, all data
R factor, R free[a]	0.25(0.31), 0.3(0.38)	0.22(0.38), 0.27(0.39)	0.23(0.37), 0.26(0.3)
B factors[b]	49.0 $Å^2$, 3.4 $Å^2$	33.0 $Å^2$, 3.1 $Å^2$	66.3 $Å^2$, 2.7 $Å^2$
Geometry[c]	0.007 Å,1.405°	0.007 Å, 1.422°	0.009 Å, 1.521°
Ramachandran[d]	87.7%/0.0%	89.0 %/0.0%	89.0 %/0.0%
Restrained NCS	0.320Å	0.100 Å	0.112 Å
PDB ID	2IUS	2IUT	2IUU

[a] Five percent of reflections were randomly selected for determination of the free R factor, prior to any refinement. R factors for the highest resolution bins are given in brackets.
[b] Temperature factors averaged for all atoms and rmsd of temperature factors between bonded atoms.
[c] Rmsds from ideal geometry for bond lengths and restraint angles.
[d] Percentage of residues in the "most favored region" of the Ramachandran plot and percentage of outliers, corresponding number of residues in brackets.

state. The displacement of 5.5 Å equates to about 1.6 bp of B-DNA, suggesting that each monomer could displace duplex DNA by a minimum of 1.6 bp every catalytic cycle, assuming that one catalytic cycle corresponds to one jaw movement.

Based on the observed conformational change, we propose a simple inchworm model for DNA translocation by an individual subunit (Figure 5B; Yarranton and Gefter, 1979; Velankar et al., 1999). The catalytic cycle of $FtsK_C$ starts with the α domain contacting the DNA backbone through a loop on the inside of the channel, whereas the β domain is disengaged from DNA. ATP binding and hydrolysis, and subsequent ADP release, induce conformational changes that drive the α jaw away from the β head and lead to the translocation of DNA by at least 1.6 bp relative to the protein. At the end of the catalytic cycle, DNA is bound more strongly through the β domain, whereas the α jaw has been pulled away from the DNA slightly and is no longer capable of binding. In this way, the two domains cycle out of phase between strong and weak contacts such that α binds DNA strongly and moves the DNA through the channel, enabling β to bind DNA strongly (so translocation is directional) while α "recovers." After a translocation step of ~1.6 bp by a single subunit with no relative rotation of protein and DNA, the helical nature of DNA dictates that that same subunit will no longer be in a position to translocate DNA further, but a neighboring protomer will be. For successive protomer steps to follow the helical nature of DNA without protein-DNA rotation, each of the six protomers needs to translocate one-sixth of the 10.5 bp/turn of the DNA helical repeat. Hence, the expected protomer step size would be 1.75 bp, which closely resembles the 1.6 bp minimal step size observed.

The direction of DNA translocation relative to the protein is unknown, but we speculate that DNA enters a hexamer from the β domain side, principally because the γ domains that interact with XerD recombinase are located on the β domain side of the ring. This translocation direction fits published data on SV40 L-Tag and archaeal MCM that show ssDNA being pumped through rings from the motor (β) domain side (Li et al., 2003; McGeoch et al., 2005).

Rotary Inchworm-Type Model of dsDNA Translocation

To investigate how individual subunits within an active FtsK ring function together, we measured $PaFtsK_{C\Delta\gamma}$ ATPase activity in the presence of increasing concentrations of a Walker A ATPase mutant $PaFtsK_{C\Delta\gamma}$ K472A (Figure 5C). This mutant protein had no ATPase activity but could form hexameric rings with a similar propensity to wild-type $PaFtsK_{C\Delta\gamma}$ (Figures 1C and 5C, middle). The ATPase activity of $PaFtsK_{C\Delta\gamma}$ decreased in a nonlinear manner as increasing proportions of mutant protein were added (Figure 5C). These data suggest that the individual subunits of a ring do not hydrolyze ATP independently of each other.

We propose a rotary inchworm model for dsDNA translocation by hexameric $FtsK_C$. (Figure 5D). A ring of $FtsK_C$ accommodates dsDNA in its central channel, with protein-DNA contacts involving one or two of the six monomers. Considering one monomer for simplicity (involvement of a second monomer per translocation step should affect only ATP consumption, not mechanistic principles), the monomer undergoes a catalytic cycle (Figure 5B) leading to the translocation of DNA through the channel by at least 1.6 bp, as described above. This translocation, with little rotation of DNA relative to protein, brings the DNA backbone into register with the DNA binding loops of the next $FtsK_C$ subunit around in the hexamer while preventing further DNA binding by the initial monomer. The second subunit undergoes a catalytic cycle, translocation occurs, and the DNA is then bound by the next subunit around. As such, there is a cycle of monomer binding around the hexamer, the helical structure of DNA enabling such a cycle to pump DNA. If DNA entered the hexamer from the β domain side, the active ATPase subunit would change around the ring in an anticlockwise manner, as one looks at a ring from the β side (as in Figure 3B, right). So that protein-DNA contacts are conserved as the homohexameric ring translocates, it is likely that the motor moves

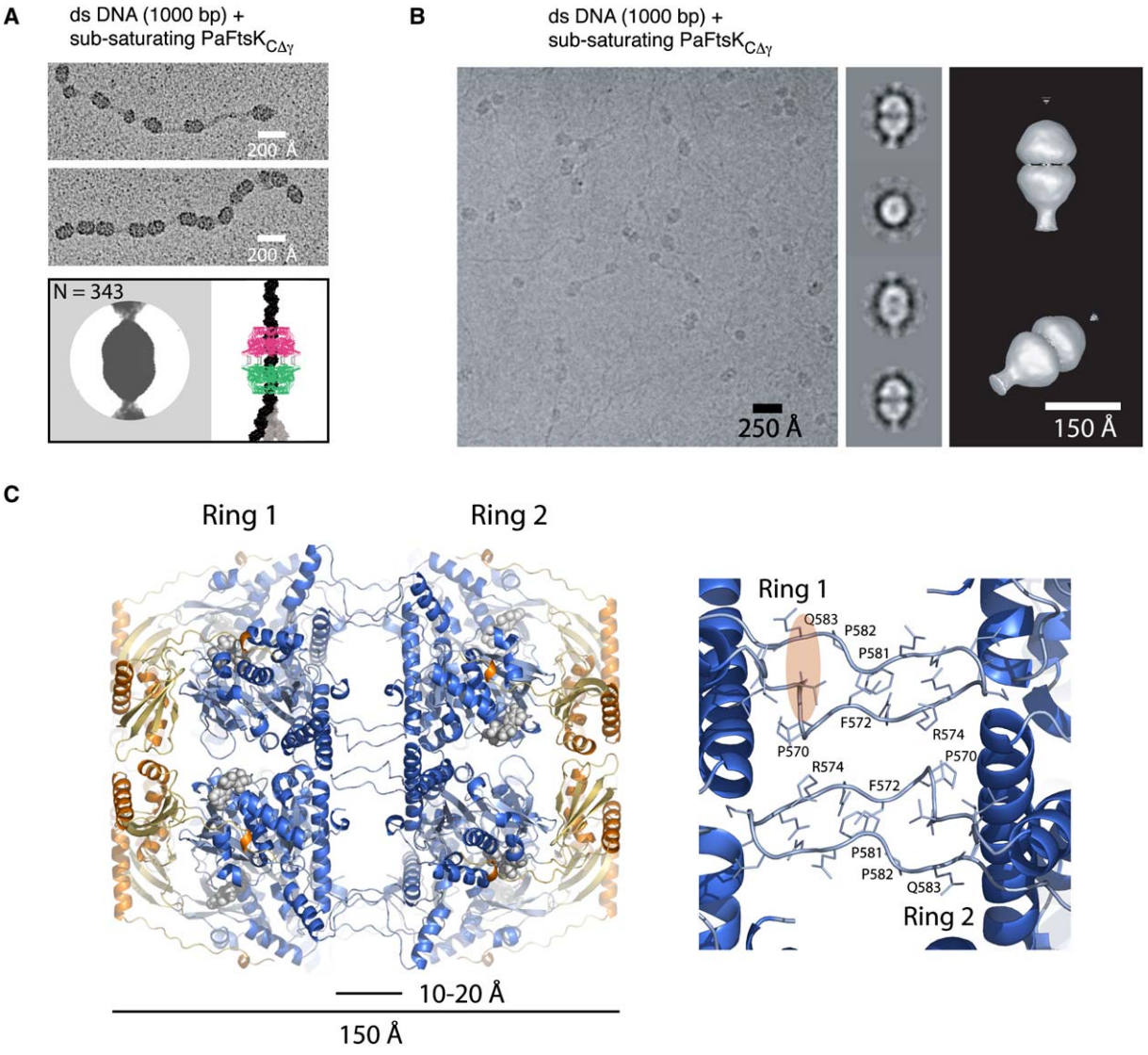

Figure 4. Double Rings of PaFtsK$_{C\Delta\gamma}$ Show DNA in the Central Pore of the Protein

(A) Visualization of subsaturating concentrations of PaFtsK$_{C\Delta\gamma}$ on dsDNA (1000 bp) by rotary shadowing and EM shows single and double rings. The average of well-separated double rings shows that DNA passes through the central hole of each hexamer (bottom left). The cartoon interpretation (bottom right) shows how the flexibility of DNA exiting the double ring can yield cone-shaped density at the end of the dodecamer in the particle average.

(B) Three-dimensional cryo-EM reconstruction of PaFtsK$_{C\Delta\gamma}$ dodecamers on DNA. Left, raw image of PaFtsK$_{C\Delta\gamma}$ dodecamers on 1000 bp DNA. Center, four examples of the class sums used to calculate the 3D model. Right, surface rendering of the final 3D cryo-EM model derived from 1024 images. To lessen the effect of DNA flexibility on the final reconstruction, the DNA was preferentially aligned to one side of the double ring.

(C) The crystals of hexameric PaFtsK$_{C\Delta\gamma}$ contain dodecamers formed by the head-to-head assembly of two 6-fold rings (left). The handle (residues 570–582 in PaFtsK) is the only part of the protein involved in hexamer-hexamer contacts (right). The pink oval highlights the residues that are linked together in the handle mutant protein (after deletion of residues 570–582).

an integral number of base pairs along the DNA every catalytic step. The figure of 1.6 bp/subunit obtained from the structures is a minimum, and so, it is likely that each catalytic step leads to a translocation along DNA of 2 bp. A translocation of 2 bp per monomer cycle enables the pump to move 12 bp per hexameric cycle. This figure fits closely with the 10.5 bp/turn dimensions of B-DNA. The extra 1.5 bp translocated per hexamer cycle would manifest as DNA supercoiling outside the complex (positive in front, negative behind), as observed in single-molecule and biochemical experiments on EcFtsK$_{50C}$ (Figure 1D; Aussel et al., 2002; Saleh et al., 2005).

The cycling of the active ATPase, and hence the active DNA binding/translocating unit, around the protein ring is sufficient for FtsK$_C$ to pump helical DNA directionally with very little net rotation of DNA relative to protein. We favor a sequential model of ATPase activity around the ring as the most likely way in which FtsK$_C$ translocation is coordinated. Each round of DNA binding and nucleotide hydrolysis/release would lead to a conformational change in that subunit, possibly moving the arginine finger (R620) into the active site of the next subunit in sequence and thereby activating it. This cycling of ATPase activity around the ring would be similar to the

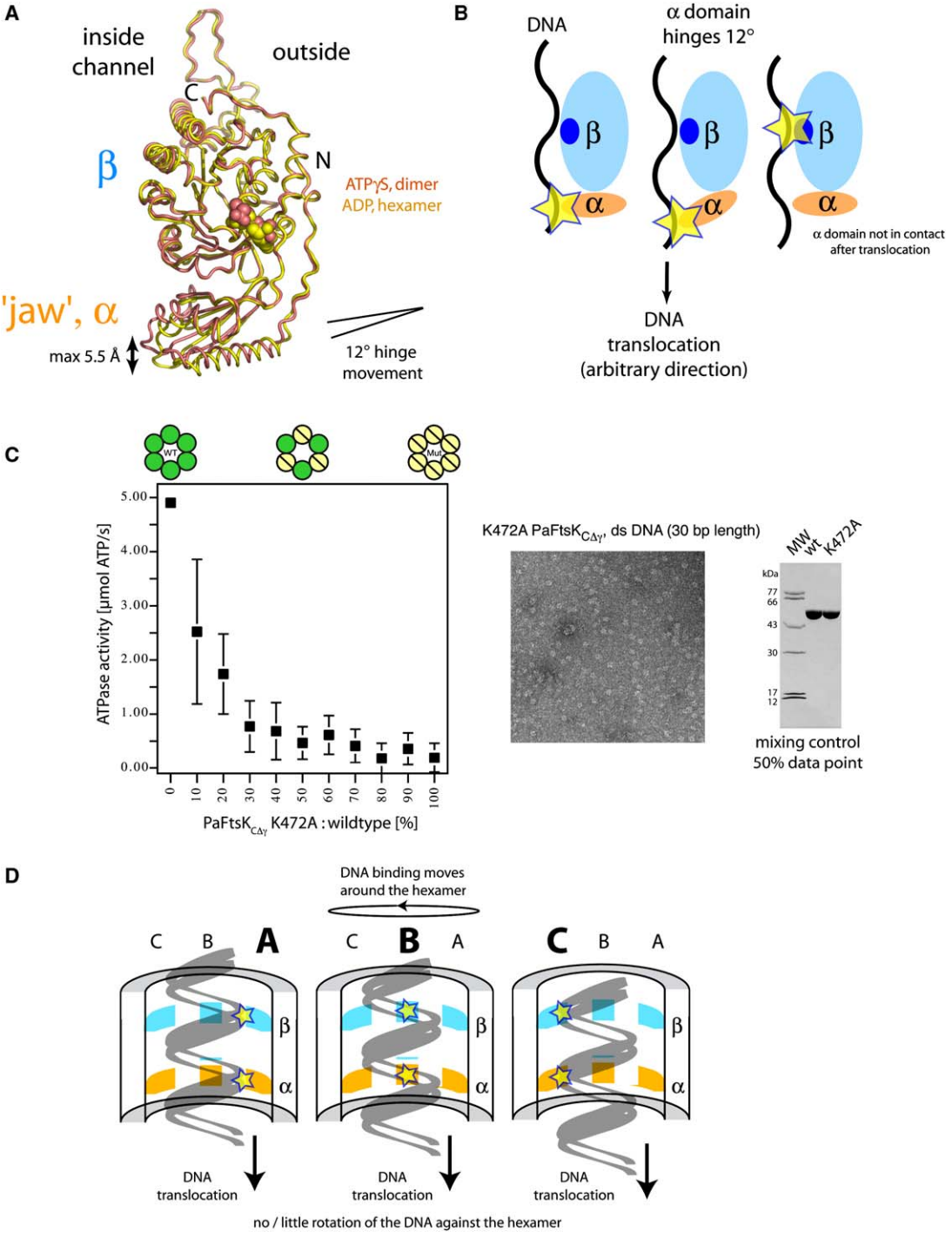

Figure 5. DNA Translocation by a Rotary Inchworm Mechanism

(A) Comparison of the crystal structures of PaFtsK$_C$ in the dimeric and hexameric forms reveals a conformational change that is a pure hinged movement of the α domain (jaw) against the β domain. This movement alters the distance between the putative DNA-contacting regions in α and β by 5.5 Å, equating to ~1.6 bp of B-DNA.

(B) Inchworm model of DNA translocation by a single subunit of FtsK$_C$. First, the α domain binds the DNA backbone (left, indicated by star). Nucleotide binding, hydrolysis or release causes a hinged movement between α and β (A), translocating the DNA downward (center). After translocation, the DNA backbone is bound by β but released from α (right). The helical nature of DNA means that the α domain of this subunit cannot interact with DNA again until a full turn has been translocated through the ring. The direction of DNA translocation shown is arbitrary.

(C) Nonlinearity of ATPase activity against mutant protein percentage indicates a sequential or concerted binding mechanism. Left, ATPase activity of wild-type PaFtsK$_{C\Delta\gamma}$ in the presence of different proportions of K472A (Walker A) mutant PaFtsK$_{C\Delta\gamma}$. Middle, negative-stain EM of the mutant protein on 30 bp dsDNA, showing that it can form hexameric rings. Right, example SDS-PAGE showing that at the 50% K472A point proteins were mixed at equal concentrations.

(D) Rotary inchworm model of DNA translocation by hexameric FtsK$_C$. Individual monomers likely translocate dsDNA in steps of 2 bp (see [B]). Within a hexameric ring, sequential cycles of ATPase activity, and hence DNA binding, around the inside of the ring (from subunits A to B to C,

model proposed for T7 gp4 helicase (Singleton et al., 2000), the ϕ12 RNA packaging motor (P4; Mancini et al., 2004; Lisal and Tuma, 2005), and the ϕ29 DNA packaging motor (Chemla et al., 2005) and would be efficient in allowing 2 bp translocation per ATP hydrolyzed.

Experimental Procedures

FtsK Expression And Purification

$FtsK_C$ from *E. coli* (residues 818–1329, K997A Walker A mutant, untagged, SWISS_PROT: FTSK_ECOLI) was expressed in BL21(DE3) *E. coli* cells. The protein was purified by using heparin, Q-Sepharose, and size-exclusion chromatography and concentrated to more than 10 mg/ml in buffer A (20 mM Tris-Cl, 1 mM EDTA, and 1 mM sodium azide, final pH 7.5). Selenomethionine-substituted protein was produced by the feedback inhibition method (van Duyne et al., 1993) and purified as above in the presence of 5 mM DTT.

C-terminally KLH_6-tagged $PaFtsK_C$ (residues 247–811 of full-length protein, 63.6 kDa, SWISS_PROT: FTSK_PSEAE) and $PaFtsK_{C\Delta\gamma}$ (247–728, 53.9 kDa), with and without handle (570–582), and $PaFtsK_C$ without any linker (304–811) were expressed in BL21(AI) *E. coli*. Proteins were purified by using nickel Sepharose HP and eluted between 5% and 30% buffer C in buffer B (buffer B: 50 mM Tris-Cl, 300 mM NaCl, final pH 7.0; buffer C: 50 mM Tris-Cl, 1 M imidazole, final pH 7.0). After ammonium sulfate precipitation (60% saturation), proteins were passed through Sephacryl S300 size exclusion columns in buffer A, further purified by using a Mono Q column, and desalted (Sephadex G25). Protein yields of 1.5–2.0 mg per liter culture were obtained. PaFtsK proteins lacking His tags were purified by Q-Sepharose, heparin, and size-exclusion chromatography. Protein identities were confirmed by using electrospray mass spectrometry.

ATPase Assays

ATPase activities were measured by spectrophotometric detection of inorganic phosphate (P_i) with malachite green reagent (1:1:2:2 ammonium molybdate (5.72%, w/v): HCl (6 N): polyvinyl alcohol (2.32%, w/v): malachite green (0.08712%, w/v), all in distilled water). Reactions (20 μl) containing ATP (1 mM), $MgCl_2$ (1 mM), dsDNA (16 bp, 50 μM bp), and PaFtsK (20 μM monomer) were mixed in 20 mM Tris-Cl (pH 7.5) and incubated at 37°C for 30′. Malachite green reagent (200 μl in 700 μl water) was added and P_i release monitored at 630 nm. In the wt/K472A mutant mixing experiment, different ratios of these proteins were mixed (in buffer A plus 200 mM NaCl; combined protein concentration of 10 μM) before being added to a final combined protein concentration of 1 μM to reactions (40 μl) containing ATP (1 mM), $MgCl_2$ (1 mM), and dsDNA (16 bp, 50 nM bp) in 20 mM Tris/HCl (pH 7.5). Assays were run (3 min, RT) in 96-well microtiter plates and samples postdiluted 1:10 with HCl (100 μl, 100 mM; to ensure readout linearity) prior to mixing with malachite green reagent (200 μl) and read out at 630 nm. Correct mixing of proteins was checked by using SDS-PAGE.

Translocation Assays

DNA translocation was measured by supercoil induction in an array of pUC19 topoisomers. DNA substrate was prepared by partial relaxation of pUC19 with *Vaccinia* virus topoisomerase. Reactions (10 μl) involved preincubating buffer (RB: 10 mM Tris-Cl, 4 mM $MgCl_2$, fixed in pH 7.5), BSA (0.1 mg/ml), relaxed pUC19 (1.4 nM), FtsK (0.5 μM monomer $EcFtsK_{50C}$; 3.0 μM monomer PaFtsK), and TopA (*E. coli*) on ice for 5 min before adding Ni-NTA beads (1 μl; Qiagen) and continuing incubation on ice for a further 5 min. ATP or AMP-PNP was then added, and the reactions were incubated at 37°C for 30 min. Reactions were stopped, deproteinized, and analyzed by 0.8% agarose gel electrophoresis.

In Vitro Recombination Assays

Reactions (10 μl) were carried out in RB plus 1 mM DTT (37°C, 30 min) essentially as described (Aussel et al., 2002). The dimer resolution substrate was pSDC124 (4.0 kbp), containing two *dif* sites in direct repeat such that Xer site-specific recombination resolves the plasmid into two smaller supercoiled plasmids (3.0 kbp and 1.0 kbp). Reactions were stopped and analyzed as per the translocation assays.

EM

Negatively stained samples were prepared on glow-discharged carbon-coated grids by using a modified deep stain (Stoops et al., 1992). Briefly, mixtures of DNA (30, 55, 161, 235, 500, or 625 bp, sequence unimportant; ~3 μM bp) and $PaFtsK_c$ (~750 nM monomer when saturating) were incubated on ice in EM buffer (EMB; 25 mM Tris-Cl, 4 mM MgOAc, and 2 mM ATPγS, fixed in pH 7.5) for up to 30 min, diluted 3-fold, and applied to grids. After 30 s, grids were rinsed with 2% uranyl acetate, blotted dry with filter paper, and further dried with a hairdryer.

Rotary shadowed samples were prepared on glow-discharged carbon-coated grids essentially as described (Williams, 1977). Mixtures of DNA (1000 bp; ~12 nM) and $PaFtsK_c$ (~2 μM monomer when saturating or ~20 nM monomer when nonsaturating) were incubated in EMB on ice for 30 min, diluted 15-fold, and applied to grids. After 30 s, grids were rinsed with 0.05% uranyl acetate, blotted with filter paper, and dried in a stream of air. Rotary shadowing was performed in an Edwards E306A coating system by using a platinum source with an oblique angle of 8° and a sample-to-source distance of 7 cm.

Images of negatively stained and shadowed samples were recorded to film on a FEI Tecnai 12 at 120 kV with −1.5 μm defocus. Negatives were scanned at 6 μm/pixel (MRC-KZA scanner). DNA length measurements were made with XIMDISP (Crowther et al., 1996). For class average analysis, automated particle picking was performed with SIGNATURE and image processing was performed with IMAGIC (van Heel et al., 1996). Two-dimensional class averages were calculated by summing similar classes from one round of classification and alignment.

Cryo-EM and Image Processing

Mixtures of DNA (1000 bp; ~60 nM) and $PaFtsK_c$ (~0.8 μM monomer) were incubated in EMB on ice (4 hr) after which samples (3.5 μl) were applied to glow-discharged Quantifoil grids. Grids were blotted with filter paper, plunge frozen in liquid ethane, and imaged with a FEI F20 microscope at 62,000× magnification with −4 to −5 μm defocus. Negatives were scanned (MRC-KZA scanner), and images of double rings (3637 particles) were boxed out with XIMDISP (Crowther et al., 1996). Image processing was performed with IMAGIC (van Heel et al., 1996). Images were first pixel-averaged 4 × 4 (to 3.9 Å/pixel), corrected for contrast transfer function, and filtered. A first 3D model containing only the double ring portion of the complex was calculated with 6-fold symmetry using several rounds of multivariate statistical analysis (MSA) and multireference alignment (MRA) with a tight mask in order to block out contributions from flexible DNA. Because the DNA exiting double rings is flexible, a second reconstruction using two rounds of MSA and MRA with the first 3D model as a reference was used to orient particles with respect to DNA signal. This led to class sums with well-aligned, strong DNA signal at only one side of the complex. A final round of MSA was used to calculate classes. The best of these classes (derived from 1024 particles) was used to calculate a final 3D reconstruction using 6-fold symmetry.

Analytical Ultracentrifugation

Equilibrium and sedimentation velocity experiments were performed in a Beckman Optima XL-A analytical ultracentrifuge with an An60-Ti rotor. Samples consisted of $PaFtsK_{C\Delta\gamma}$ (up to 20 μM monomer) in RB, supplemented with ATPγS (1 mM), MgOAc (2 mM), and dsDNA (15 bp, 4 μM) as required. Sedimentation velocity was 50,000 rev/min, with scans of the single cell taken every 1.5 min. Adjacent sets of data were analyzed by using the DCDT software (Philo, 2000).

active subunit indicated by stars) enable the continuous translocation of DNA downward. The helical nature of DNA and the cycling of monomer activity around the ring mean that there is little rotation of the DNA relative to the protein channel. The direction of translocation is as in (B) and has been chosen arbitrarily.

Crystallization

All initial crystallization conditions were found by using our in-house 100 nl high-throughput crystallization setup employing 1500 standard conditions (Stock et al., 2005). Final drops consisted of 1 μl protein (~200 μM monomer) and 1 μl reservoir solution. $EcFtsK_C$ SeMet was crystallized with reservoir solution containing 0.1 M Tris-Cl (pH 7.5) and 3 M NaCl. Crystals were cryoprotected with 44% ethylene glycol, which reduces twinning and lowers symmetry to $P3_2$. $EcFtsK_C$ was crystallized by using reservoir solution containing 0.1 M imidazole-Cl (pH 7.7), 0.3 M calcium acetate, 0.02 M fresh cysteine, and 8% (w/v) PEG 2000. Cryoprotectant: 20% PEG 550 MME in reservoir solution.

$PaFtsK_C$ was crystallized with 0.1 M imidazole-Cl (pH 7.0), 0.07 M calcium acetate, and 28% (w/v) PEG 300, and the protein solution also contained ATPγS (2 mM) and MgOAc (4 mM). Cryoprotectant: 45% (w/v) PEG 300 in reservoir solution. $PaFtsK_{C\Delta\gamma}$ was crystallized as a hexamer in the presence of ATPγS (2 mM) and MgOAc (4 mM) with reservoir solution containing 0.1 M Tris-Cl (pH 7.5) and 1.4 M ammonium phosphate. Cryoprotectant: 25% (w/v) glycerol in reservoir solution. All crystals were grown at 19°C.

Structure Determination

Datasets were integrated by using MOSFLM and reduced using SCALA (CCP4, 1994: Table 1). Molecular replacement and refinement were performed by using CNS version 1.1 (Brunger et al., 1998).

De novo structure determination of $FtsK_C$ was performed on Se-Met-substituted crystals of $EcFtsK_C$. The crystals contained six molecules per asymmetric unit when using high percentage ethylene glycol cryobuffer and were twinned with $\alpha = 0.35$, twin operator $h + k, -k, -l$. The true space group is $P3_2$. Shake 'n Bake (Smith et al., 1998) found 30 sites, and after 6-fold averaging and phase extension, a high-quality map could be achieved for manual building. A partially refined model was then used to place six $FtsK_C$ monomers in the native EcFtsK dataset (space group $P2_1$) by using PHASER (Storoni et al., 2004). PHASER was also used to solve the $PaFtsK_C$ structure in space group P1 at 2.25 Å resolution. The CNS-refined $PaFtsK_C$ model was then used to place six molecules in the $P2_1$ $PaFtsK_{C\Delta\gamma}$ dataset by using PHASER, arranged in a closed circular hexameric structure with one hexamer per asymmetric unit.

Supplemental Data

Supplemental Data include Supplemental Experimental Procedures, Supplemental References, and one figure and can be found with this article online at http://www.molecule.org/cgi/content/full/23/4/457/DC1/.

Acknowledgments

We thank P. Jonathan Butler (MRC-LMB) for performing the ultracentrifugation experiment, Rachel Baker (Oxford) for EcFtsK γ domain purification, and Sonia Trigueros (Oxford) for help with the translocation assay. J.Y. was supported by an Medical Research Council studentship. Further support was provided by grants from the Wellcome Trust (GR068713MA) and Human Frontier Science Program (RGP0001/2003-C). It is our pleasure to acknowledge great support on the following beamlines: ID29, BM14, ID14eh1, and ID14eh4 (European Synchrotron Radiation Facility, Grenoble, France).

Received: October 21, 2005
Revised: May 15, 2006
Accepted: June 13, 2006
Published: August 17, 2006

References

Aussel, L., Barre, F.-X., Aroyo, M., Stasiak, A., Stasiak, A.Z., and Sherratt, D.J. (2002). FtsK is a DNA motor protein that activates chromosome dimer resolution by switching the catalytic state of the XerC and XerD recombinases. Cell *108*, 195–205.

Barre, F.-X., Aroyo, M., Colloms, S.D., Helfrich, A., Cornet, F., and Sherratt, D.J. (2000). FtsK functions in the processing of a Holliday junction intermediate during bacterial chromosome segregation. Genes Dev. *14*, 2976–2988.

Bath, J., Wu, L.J., Errington, J., and Wang, J.C. (2000). Role of *Bacillus subtilis* SpoIIIE in DNA transport across the mother cell-prespore division septum. Science *290*, 995–997.

Ben-Yehuda, S., Rudner, D.Z., and Losick, R. (2003). Assembly of SpoIIIE DNA translocase depends on chromosome trapping in Bacillus subtilis. Curr. Biol. *13*, 2196–2200.

Bigot, S., Corre, J., Louarn, J.M., Cornet, F., and Barre, F.-X. (2004). FtsK activities in Xer recombination, DNA mobilization and cell division involve overlapping and separate domains of the protein. Mol. Microbiol. *54*, 876–886.

Bigot, S., Saleh, O.A., Lesterlin, C., Pages, C., El Karoui, M., Dennis, C., Grigoriev, M., Allemand, J.-F., Barre, F.-X., and Cornet, F. (2005). KOPS: DNA motifs that control E. coli chromosome segregation by orienting the FtsK translocase. EMBO J. *24*, 3770–3780.

Boyle, D.S., Grant, D., Draper, G.C., and Donachie, W.D. (2000). All major regions of FtsK are required for resolution of chromosome dimers. J. Bacteriol. *182*, 4124–4127.

Brunger, A.T., Adams, P.D., Clore, G.M., DeLano, W.L., Gros, P., Grosse-Kunstleve, R.W., Jiang, J.S., Kuszewski, J., Nilges, M., Pannu, N.S., et al. (1998). Crystallography & NMR system: a new software suite for macromolecular structure determination. Acta Crystallogr. D Biol. Crystallogr. *54*, 905–921.

Capiaux, H., Cornet, F., Corre, J., Guijo, M.-I., Pérals, K., Rebollo, J.E., and Louarn, J.-M. (2001). Polarization of the *Escherichia coli* chromosome. A view from the terminus. Biochimie *83*, 161–170.

CCP4 (Collaborative Computational Project, Number 4) (1994). The CCP4 suite: programs for protein crystallography. Acta. Crystallogr. D. Biol. Crystallogr. *50*, 760–763.

Chemla, Y.R., Aathavan, K., Michaelis, J., Grimes, S., Jardine, P.J., Anderson, D.L., and Bustamante, C. (2005). Mechanism of force generation of a viral DNA packaging motor. Cell *122*, 683–692.

Crowther, R.A., Henderson, R., and Smith, J.M. (1996). MRC image processing programs. J. Struct. Biol. *116*, 9–16.

Fletcher, R.J., Bishop, B.E., Leon, R.P., Sclafani, R.A., Ogata, C.M., and Chen, X.S. (2003). The structure and function of MCM from archaeal *M. Thermoautotrophicum*. Nat. Struct. Biol. *10*, 160–167.

Gomis-Rüth, F.X., Moncalian, G., Perez-Luque, R., Gonzalez, A., Cabezon, E., de la Cruz, F., and Coll, M. (2001). The bacterial conjugation protein TrwB resembles ring helicases and F1-ATPase. Nature *409*, 637–641.

Holm, L., and Sander, C. (1995). Dali: a network tool for protein structure comparison. Trends Biochem. Sci. *20*, 478–480.

Ip, S.C., Bregu, M., Barre, F.-X., and Sherratt, D.J. (2003). Decatenation of DNA circles by FtsK-dependent Xer site-specific recombination. EMBO J. *22*, 6399–6407.

Iyer, L.M., Leipe, D.D., Koonin, E.V., and Aravind, L. (2004). Evolutionary history and higher order classification of AAA+ ATPases. J. Struct. Biol. *146*, 11–31.

Krishna, T.S., Kong, X.P., Gary, S., Burgers, P.M., and Kuriyan, J. (1994). Crystal structure of the eukaryotic DNA polymerase processivity factor PCNA. Cell *79*, 1233–1243.

Li, D., Zhao, R., Lilyestrom, W., Gai, D., Zhang, R., DeCaprio, J.A., Fanning, E., Jochimiak, A., Szakonyi, G., and Chen, X.S. (2003). Structure of the replicative helicase of the oncoprotein SV40 large tumour antigen. Nature *423*, 512–518.

Lisal, J., and Tuma, R. (2005). Cooperative mechanism of RNA packaging motor. J. Biol. Chem. *280*, 23157–23164.

Liu, G., Draper, G.C., and Donachie, W.D. (1998). FtsK is a bifunctional protein involved in cell division and chromosome localization in *Escherichia coli*. Mol. Microbiol. *29*, 893–903.

Mancini, E.J., Kainov, D.E., Grimes, J.M., Tuma, R., Bamford, D.H., and Stuart, D.I. (2004). Atomic snapshots of an RNA packaging motor reveal conformational changes linking ATP hydrolysis to RNA translocation. Cell *118*, 743–755.

Massey, T.H., Aussel, L.A., Barre, F.-X., and Sherratt, D.J. (2004). Asymmetric activation of Xer site-specific recombination by FtsK. EMBO Rep. *5*, 399–404.

McGeoch, A.T., Trakselis, M.A., Laskey, R.A., and Bell, S.D. (2005). Organization of the archaeal MCM complex on DNA and implications for the helicase mechanism. Nat. Struct. Mol. Biol. *12*, 756–762.

Niedenzu, T., Roleke, D., Bains, G., Scherzinger, E., and Saenger, W. (2001). Crystal structure of the hexameric replicative helicase RepA of plasmid RSF1010. J. Mol. Biol. *306*, 479–487.

Patel, S.S., and Picha, K.M. (2000). Structure and function of hexameric helicases. Annu. Rev. Biochem. *69*, 651–697.

Pease, P.J., Levy, O., Cost, G.J., Gore, J., Ptacin, J.L., Sherratt, D., Bustamante, C., and Cozzarelli, N.R. (2005). Sequence-directed DNA translocation by purified FtsK. Science *307*, 586–590.

Philo, J.S. (2000). A method for directly fitting the time derivative of sedimentation velocity data and an alternative algorithm for calculating sedimentation coefficient distribution functions. Anal. Biochem. *279*, 151–163.

Saleh, O.A., Pérals, C., Barre, F.-X., and Allemand, J.-F. (2004). Fast, DNA-sequence independent translocation by FtsK in a single molecule experiment. EMBO J. *23*, 2430–2439.

Saleh, O.A., Bigot, S., Barre, F.-X., and Allemand, J.-F. (2005). Analysis of DNA supercoil induction by FtsK indicates translocation without groove-tracking. Nat. Struct. Mol. Biol. *12*, 436–440.

Singleton, M.R., Sawaya, M.R., Ellenberger, T., and Wigley, D.B. (2000). Crystal structure of T7 gene 4 ring helicase indicates a mechanism for sequential hydrolysis of nucleotides. Cell *101*, 589–600.

Smith, G.D., Nagar, B., Rini, J.M., Hauptman, H.A., and Blessing, R.H. (1998). The use of SnB to determine an anomalous scattering substructure. Acta Crystallogr. D Biol. Crystallogr. *54*, 799–804.

Stock, D., Peristic, O., and Löwe, J. (2005). Robotic nanolitre protein crystallography at the MRC Laboratory of Molecular Biology. Prog. Biophys. Mol. Biol. *88*, 311–327.

Stoops, J.K., Kolodziej, S.J., Schroeter, J.P., Bretaudiere, J.P., and Wakil, S.J. (1992). Structure-function relationships of the yeast fatty acid synthase: negative-stain, cryo-electron microscopy, and image analysis studies of the end views of the structure. Proc. Natl. Acad. Sci. USA *89*, 6585–6589.

Storoni, L.C., McCoy, A.J., and Read, R.J. (2004). Likelihood-enhanced fast rotation functions. Acta Crystallogr. D Biol. Crystallogr. *60*, 432–438.

van Duyne, G.D., Standaert, R.F., Karplus, P.A., Schreiber, S.L., and Clardy, J. (1993). Atomic structures of the human immunophilin FKBP-12 complex with FK506 and rapamycin. J. Mol. Biol. *229*, 105–124.

van Heel, M., Harauz, G., Orlova, E.V., Schmidt, R., and Schatz, M. (1996). A new generation of the IMAGIC image processing system. J. Struct. Biol. *116*, 17–24.

Velankar, S.S., Soultanas, P., Dillingham, M.S., Subramanya, H.S., and Wigley, D.B. (1999). Crystal structures of complexes of PcrA DNA helicase with a DNA substrate indicate an inchworm mechanism. Cell *97*, 75–84.

Wang, X., Possoz, C., and Sherratt, D. (2005). Dancing around the divisome: asymmetric chromosome segregation in Escherichia coli. Genes Dev. *19*, 2367–2377.

Williams, R.C. (1977). Use of polylysine for adsorption of nuclei acids and enzymes to electron microscope specimen films. Proc. Natl. Acad. Sci. USA *74*, 2311–2315.

Yarranton, G.T., and Gefter, M.L. (1979). Enzyme-catalyzed DNA unwinding: studies on *Escherichia coli* rep protein. Proc. Natl. Acad. Sci. USA *76*, 1658–1662.

Yates, J., Aroyo, M., Sherratt, D.J., and Barre, F.-X. (2003). Species specificity in the activation of Xer recombination at *dif* by FtsK. Mol. Microbiol. *49*, 241–249.

Yates, J., Zhekov, I., Baker, R., Eklund, B., Sherratt, D.J., and Arciszewska, L.K. (2006). Dissection of a functional interaction between the DNA translocase, FtsK, and the XerD recombinase. Mol. Microbiol. *59*, 1754–1766.

Yu, X.-C., Weihe, E.K., and Margolin, W. (1998). Role of the C-terminus of FtsK in *Escherichia coli* chromosome segregation. J. Bacteriol. *180*, 6424–6428.

Accession Numbers

Coordinates have been deposited in the Protein Data Bank under accession codes 2IUS, 2IUT, and 2IUU (Table 2).